Universality class for loopless invasion percolation models and a percolation avalanche burst model for hydraulic fracturing

Ronaldo Ortez,[1,*] John B. Rundle,[1,2,3,†] and Donald L. Turcotte[4,‡]
[1]*Department of Physics, University of California, Davis, California 95616, USA*
[2]*Department of Earth and Planetary Science, University of California, Davis, California 95616, USA*
[3]*Santa Fe Institute, Santa Fe, New Mexico 87501, USA*
[4]*Department of Geology, University of California, Davis, California 95616, USA*

(Received 21 February 2020; accepted 7 September 2020; published 22 January 2021)

Invasion percolation is a model that was originally proposed to describe growing networks of fractures. Here we describe a loopless algorithm on random lattices, coupled with an avalanche-based model for bursts. The model reproduces the characteristic *b*-value seismicity and spatial distribution of bursts consistent with earthquakes resulting from hydraulic fracturing ("fracking"). We test models for both site invasion percolation and bond invasion percolation. These have differences on the scale of site and bond lengths l. But since the networks are characterized by their large-scale behavior, $l \ll L$, we find small differences between scaling exponents. Though data may not differentiate between models, our results suggest that both models belong to different universality classes.

DOI: 10.1103/PhysRevE.103.012310

I. INTRODUCTION

Invasion percolation (IP) was proposed in Ref. [1] as a model for the displacement of one fluid in a porous medium by another "invading" fluid. It has since been applied to a variety of other dynamical processes including drainage [2], magnetic depinning of domain walls [3], contact line motion [4], and propagation of crack fronts [5].

Though all these examples have radically different small-scale behavior, their large-scale statistics reveal the universality of how the inherent randomness of each system grows to dominate their respective critical phases. Hydraulic fracturing (HF) is a similar process. During HF, low-viscous, high-pressure fluid is pumped into porous rock which produces a network of fractures within the deep, thin reservoirs. Previous studies have made attempts to characterize this fracture network for purposes of efficient gas extraction [6,7].

More recently, studies have shown significant increased seismicity in regions previously seismically inactive [8,9]. They attribute HF as the likely candidate. This is not altogether surprising since fracking is somewhat analogous to steam production via geothermal pumping. Here steam is generated by injecting fluid into the geothermal fields. In doing so, the fluid injected into basin sediments interacts with the ambient stress fields to nucleate earthquakes [10] in much a similar way.

A key feature of IP is that networks grow according to random percolation (RP) near the critical point. Critical systems are described by a family of critical exponents which characterize all aspects of the system. These power laws arise from a system having no characteristic length scale and therefore becomes symmetric under scale transformations. We observe that in classical, tectonic seismicity essentially all of the statistical properties are described by a power law: Magnitude frequency distribution (G-R magnitude scale) [11], temporal aftershock clustering (Omori aftershock law) [12], and the two-point correlation distribution [13]. In hydraulic fracturing and geothermal injection, studies show power laws describing both the magnitude-frequency distribution and two-point correlation function [14]; therefore, we believe much of the observed seismicity is well described as a system near a critical point.

Previous authors have noted the self-similar and invariant properties present in rock fractures [10], and since naturally occurring porous structures are well described by a lattice of sites connected by bonds [15], we choose to model the pumping of high-pressure, low-viscosity fluid into the sediment as a modified invasion percolation (IP) process. Here single phase liquid invades sediment by propagating through bonds adjoining sites in a two-dimensional (2D) $N \times N$ square lattice. The result is a percolation network that is self-similar and scale invariant. Aki initially proposed using the fractal dimension, D_f, of a network to determine the power-law Gutenber-Richter b parameter that characterizes the associated seismicity arising from the fracture network [16].

The observed magnitude-frequency distribution of induced seismic events differs from those localized in tectonic fault environments having Gutenberg-Richter b value near 1 [17]. Instead, a range of b values (1.2–1.5) have been observed [18]. Rather than the traditional fault slip mechanisms hosted in regions tectonically active, this kind of induced seismicity can occur in regions absent major fault structures. This suggest different universality classes describe tectonic and induced seismicity. These differences in part correspond to a different fracture mechanism for induced seismicity which is better described as the rapid reopening of the preexisting fracture network and the disturbance of the local stress field [6]. If the

*raortez@ucdavis.edu
†rundle@ucdavis.edu
‡dlturcotte@ucdavis.edu

TABLE I. A comparison of percolation models considered in this paper. Random percolation (RP) and invasion percolation (IP) are both percolation models which generate percolating clusters. We consider variants of IP. Loopless(L) invasion percolation model coupled with the avalanche burst mechanics is the model we propose in this paper. We distinguish it from the regular variant [1] and the nontrapping(NT) variant [7] since the clusters in those models are clusters of the defending fluid. Our LIP model considers clusters and bursts of invading fluid. All IP models have bond or site variants corresponding to whether the random weights are bond strengths or site sizes.

Percolation Models			
Percolation	RP		Quasi-static network growth ideal for describing medium properties. Natural clusters. No dynamic burst cluster growth.
	IP	L	Critical single phase injection with no defending fluid(or highly compressible). Critical burst growth and cluster formulation for the invading fluid.
		NT	Critical nontrapping multiphase fluid propagation with natural clusters for incompressible defending fluid. No burst or clustering for invading fluid.
		Reg	Critical network growth for multiphase injection with clustering for compressible defending fluid. No burst or clustering for invading fluid.

newly fractured network mostly follows preexisting natural fractures which themselves were the result of high-pressure oil and gas escaping and fracturing the reservoir, then we hypothesize HF as a fundamentally drainage process. Therefore, a network grown by IP should be appropriate.

Table I shows the landscape of percolation models we discuss in this paper and where our model fits. When percolation was introduced it was intended to simulate the quasistatic movement of fluid through a porous matrix driven by capillary forces. Such a model is better suited to describe the static properties of a medium. In our case, the fluid is driven by large pressure gradients generated by the HF process, and we therefore advocate going beyond static network measures like the fractal dimension (and those similar to Aki) and implementing burst dynamics into our IP algorithms to describe induced microseismicity. In addition hydrodynamic considerations suggest a loopless network is appropriate [19]. Therefore, we adopt a similar loopless bond IP network as in Ref. [20] (except here we also compare with site IP) but grow the network using our own avalanche-burst model (discussed in Sec. IV). With these added dynamics to the percolation network, we are able to produce power-law burst-frequency distributions which have scaling exponent, $\tau = 1.53$, larger than 1, and falls in the range observed in induced seismicity.

In percolation models which represent porous sediment by a lattice of sites adjoined by bonds, the precise interactions at the fluid boundaries is a function of the pore size and the capillary throat diameter. We therefore consider two loopless invasion percolation models (LIP) corresponding to the two limits: If the throat sizes are smaller than all the pores, then the fluid will tend to become trapped in the larger pores. In this limit, the pore sizes govern the motion of the invading fluid. In our simulations we would need to assign strengths to pores representing the pore size and such a model would be site invasion percolation (SIP).

In the other limit where the throat sizes dominates the flow of fluid (for example, throat sizes are small compared to pore size restricting flow) we would instead assign strengths to the bonds or throats representing the bond size and such a model would be bond invasion percolation (BIP). Initially, we imagined fracking as being necessarily a drainage process since the invader would have most difficulty with the smallest constrictions, thereby making BIP the appropriate choice. However, since the algorithms are characterized using their global properties, we may be insensitive to the details down to the bond site scale.

This then becomes a question of whether SIP and BIP share the same universality class. The literature seems to conflict on the this point. It was originally argued that SIP and BIP belong to the same universality class [21] but later it was argued that important differences arise between the two [19,22]. Here we perform a careful study of the two, illustrating the differences on the small scale, and we find that on the largest of scales, there remains a significant difference in fractal dimension D_f, though other scaling exponents remain similar. These results suggest the two processes belong to different universality classes.

Being able to distinguish between these two processes serves to illustrate the kind of sensitivity we can expect with this approach as each corresponds to different small-scale processes. Ultimately, our choice to model HF as critical phenomena necessarily restricts the phenomenology we consider. From the theory of critical behavior, the critical point is a region of phase space where the typical small-scale physics which governs much of the potential behavior becomes dominated by the inherent random fluctuations which are allowed to grow to all scales of the system [23]. In this paper we investigate which model of randomness is appropriate for the inherent randomness of HF and by which method the randomness grows to all scales.

To Summarize Our Results

Because the appropriate model for randomness in HF is unclear, we begin by comparing the simplest motivated models: Loopless site invasion percolation (LSIP) and loopless bond invasion percolation (LBIP). We are interested in determining if there are significant differences in the critical exponents of these two models. If differences do exist, then we may be able to gain insight into the details of fluid displacement on the pore or bond scale since each process has different mechanism for fluid displacement. We find that on the scale of lattice spacing there are significant differences in networks between LSIP and LBIP. However, as the scale approaches that of a very large lattice ($10^4 \times 10^4$ for example), their difference in scaling exponents D_f, $D_{\min}$, and τ is still significant but be-

come smaller. Because both models still produce sufficiently similar networks and our constraining data are limited, neither is preferred for modeling the fracture networks produced during hydraulic fracturing. Still, the small differences between the two models are significant enough to suggest they are described by different universality classes, and a sufficiently careful characterization of observed critical exponents could shed light into a more appropriate detailed small-scale model.

II. SIMULATION ALGORITHM

The invasion begins at the center with a seed site and grows through the lattice following a principle of least resistance until reaching the lattice boundary. Since this is not a multiphase flow problem (we treat the defending gas as highly compressible) we do not concern ourselves with complications like trapping. Further, since our model is loopless, we will never have any trapped regions in the traditional sense. We first describe how we simulate SIP, which essentially amounts to maintaining two list: The first is a list of filled sites, S_f, and second is a list of nearest-neighbor sites to all filled sites, S_{nn}.

(1) The invasion begins at the center of the lattice with a seed site corresponding to the injection site. (2) The seed site's four nearest neighbors are added to the list of available sites, S_{nn}. This list will be updated serving as the list of "invadable" sites during each iteration. (3) At each iteration, all new elements to S_{nn} are assigned a number from a random uniform distribution between (0,1) representing the site's strength. The list of "invadable" sites along with its strength is called the percolation front. (4) The site with the lowest strength in the percolation front is invaded and added to the list of filled sites, S_f. (5) The invaded site is removed from the percolation front ensuring it cannot be invaded multiple times. (6) The new nearest-neighbor sites to the freshly filled site is added to the list of available sites, S_{nn}. (7) Repeat (3)–(6) until reaching the lattice boundary or until reaching the desired number of invaded sites.

Most of the computation time comes in searching the percolation front at each iteration for the weakest site. Considering that each iteration changes the percolation front at most by three values, as the percolation front grows the amount of change at each iteration is small, therefore searching the list each iteration becomes highly inefficient. Instead, we maintain an ordered list which is simply updated with the new available sites at each iteration in their respective order. One then only needs to pick the first element of the list at each iteration. Even though we are assigning strengths to the sites we can still infer the path taken from site to site. This inferred network is similar to that created by assigning strengths to all bonds.

However, there is a key difference. Since this algorithm never advances by going from an occupied site to another occupied site, the inferred bond network will always be loopless. This is desirable feature for us, since pressure gradients drive the fluid from filled sites to empty sites. If two neighboring sites are filled, then no pressure gradient between them exists, so the bond between the sites should never be allowed to break. The bond network inferred by SIP naturally implements this physical condition.

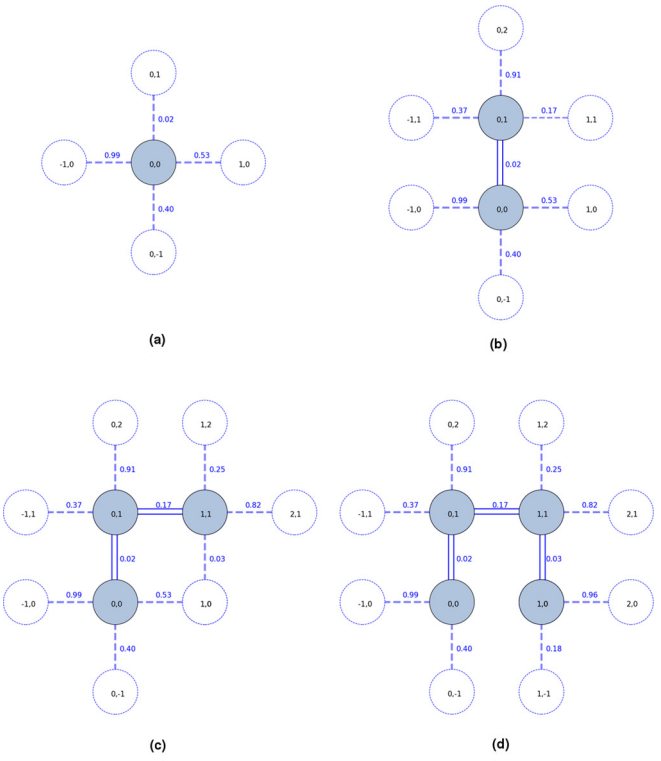

FIG. 1. Bond invasion percolation algorithm illustration. (a) A seed site is chosen in the center of the square lattice. The four nearest neighbors are added to the percolation front with random strengths between (0,1) assigned to the bonds adjoining available sites. (b) The bond with the smallest value is broken and the adjoining site is filled and added to the cluster. New values are assigned to the bonds adjoining nearest neighbors to the freshly invaded site. (c) Weakest bond again breaks adding the filled site to the cluster and assigning bond strengths connecting new nearest neighbors. (d) Loopless condition is enforced by removing all unbroken bonds joining to filled sites. Bond joining (0,0) and (1,0) is removed in this example.

Next, in order to simulate BIP we need only make a minor tweak to the SIP algorithm. Figure 1 shows an example of how BIP might proceed. If we instead assign the strengths to the sites, then we see that we can largely preserve a one-to-one correspondence between a site being invaded and the bond that must have broke. However, if we look at Fig. 1(c), then we see that there should be two bonds which can break and cause site (1,0) to be invaded. These bonds correspond to bonds $(0,0) \rightarrow (1,0)$ and $(1,1) \rightarrow (1,)$ with strength 0.53 and 0.03, respectively. In SIP, since each site is only allowed to have a single value, there will only ever be one opportunity for site (1,0) to break.

To perform BIP we can still assign values to sites, but sites must be allowed to take on multiple values. Since the numbers were assigned randomly, we can randomly choose which bond broke. By doing this we can preserve one-to-one correspondence between a site being invaded and the associated bond which broke. Further, because the cluster can only grow by invading an unfilled site, we do not need to implement additional logic to ensure loops in the bond network do not arise. The bond in joining sites (0,0) and (1,0) in Fig. 1(d) will never be allowed because those sites are already filled.

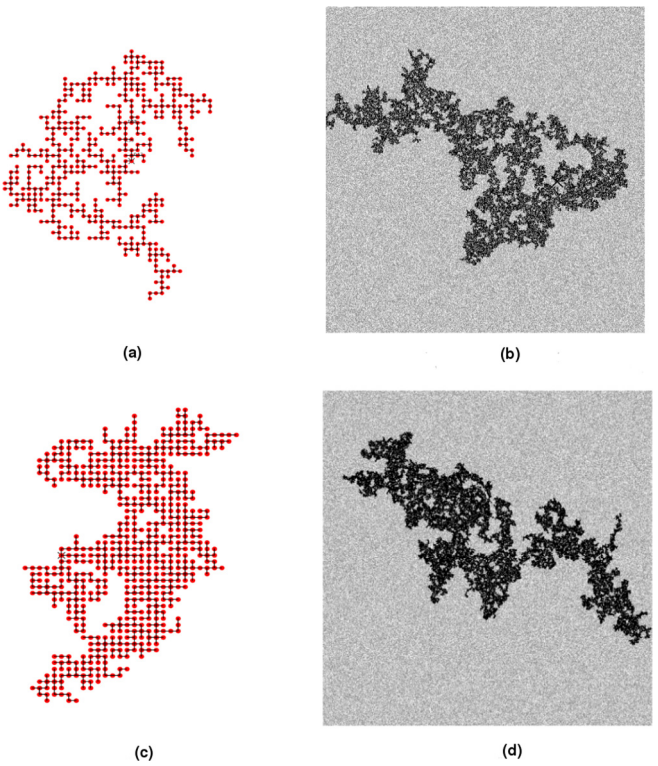

FIG. 2. Examples of LSIP (top) and LBIP (bottom) at different scales. On the left is an example of a lattice size of ∼50 × 50 and the right is 2000 × 2000. LBIP seems to be much more compact on smaller scales, but this difference becomes less noticeable at larger scales.

Fig. 2 shows clusters generated by the two algorithms (LSIP, LBIP) at different scales. Because the networks produced are loopless, we can apply to our clusters much of the rich theory associated with trees. This is also very convenient and insightful way to store the percolation clusters because it in many ways reflects the self-similar structure of the percolation cluster. We implement a recursive algorithm to create a tree data structure that reproduces the connectedness of the sites in our percolation clusters. Not only is this a natural way to represent our clusters but it allows one to quickly traverse the various paths through the cluster, which is key since traditional path finding algorithms can be more computationally expensive than creating the entire cluster. With a tree structure and a recursive path finding algorithm we can efficiently extract the path characterization to further characterize the network of our algorithms.

We also utilize the tree structure in defining and characterizing our avalanche burst model. We discuss this in more detail in Sec. IV, but quickly, our burst model defines a burst to be all connected sites which sequentially break below some threshold strength. Since we can produce different burst statistics by changing the threshold while using the same tree, we can more efficiently characterize the affects of our burst model. By changing the burst threshold we merely change how the root tree is broken down into sets of subtrees where each subtree represents a burst. This takes less time than creating a cluster grown by bursts with a particular threshold each time to generate burst statistics for a different thresholds.

III. NETWORK CHARACTERIZATION

Following traditional percolation theory we characterize networks through various scaling relations. Initially, it was argued that the scaling relations would be insensitive to whether or not one simulated bond or site percolation [15], and thus they would fall under the same universality class. More recent work has called this into question [19].

In this work,we highlight the difference between BIP and SIP and the changes one must make to SIP to reproduce BIP. In effect, it supports the more recent work finding differences in the scaling relations between the two and suggests they should belong to different universality classes. Still, the significance of universality classes is somewhat undermined because even if they did belong to the same universality classes, the universality would be broken depending on whether or not an IP model is trapping or nontrapping. Much of the literature focuses on two phase dynamics (the displacement of one fluid by another) which makes the trapping variety more appropriate. We focus on the invasion of a fluid into an empty lattice, so we opt for the less common nontrapping variety.

The first and perhaps most important scaling relation is the fractal dimension of the network. If the number of filled sites represents the mass of a cluster, then its mass should scale according to the following relation:

$$M(L) \sim L^{D_f}, \tag{1}$$

where D_f is called the fractional or fractal dimension. There are multiple techniques for determining the fractal dimension of the sample spanning cluster (SSC). The standard approach in the literature relies on counting the number sites within circles of increasing radii with a fixed center [24]. Norris *et al.* [20] relied on a similar technique, but rather than randomly choosing the center of the set of circles to be random sites within the SSC, they chose the injection site to be the center and averaged the counts over many clusters (1000) with fixed mass (m = 100 million). These results are possibly somewhat problematic because they do not properly factor in finite-size effects. Moreover, the fractal dimension should not depend on the choice of the center (which is why Reference [24] argued for taking an average over many choices). References [25,26] used a technique similar to before, but instead defined a local fractal dimension, $D_f(M)$ which follows from Eq. (1),

$$D_f(M) \equiv \frac{d\log M}{d\log L}, \tag{2}$$

and estimate how this function approaches the asymptotic value of in the infinite limit.

Since periodic boundary conditions are not implemented and because both previous work [20] and our models take the center to be sole injection point, the fractal dimensions of the clusters are more affected by finite-size issues. The effect is especially pronounced if one percolates the cluster within a lattice of fixed size rather than percolating clusters up to a set mass.

With these considerations, we used a box counting technique(more commonly used in fractal dimension studies) to determine the mass scaling, and generated clusters with fixed mass rather than fixed lattice size. Moreover, rather than a

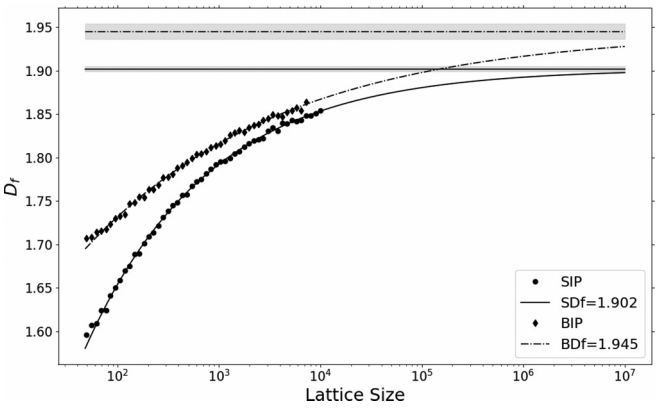

FIG. 3. The behavior of the local fractal dimension $D_f(M)$ as defined by (2) for LSIP (solid) and LBIP (dash dotted). We compute an ensemble average $\langle D_f(M)\rangle$ for lattices in the range $[50, 10^4]$ and fit the results to an exponential function via minimization of least squares. We determine the asymptote of each curve from the fit and the gray region around the asymptotes indicates the error in asymptopte fit parameter.

simple linear fit, we use the approach of Refs. [25,26] to determine how the local fractal dimension approaches its asymptotic limit. Finite-size scaling theory argues that at criticality the correlation length of the system becomes infinite. This means there is only one fundamental length scale to the system. Since the mass scales with L according to some power law, the mass itself should also follow a power law. This leads to the following assertion:

$$|D - D_f(M)| \equiv M^{\omega}, \tag{3}$$

where local fractal dimension, $D_f \to D_f(M)$ in the infinite mass limit. If we plug (1) into (2) we get the following differential equation (approach asymptotic value from below):

$$\frac{d\log M}{d\log L} = -CA^{-\omega}L^{-\omega D_f} + D_f. \tag{4}$$

The solution of which is found to be of the form:

$$\log M = \frac{c0}{\omega Df}L^{-\omega D_f} + D_f \log L + c1, \tag{5}$$

where $c0, c1$ are constants. If we perform a log-log plot then the first term is the nonlinear correction. This can be compared to what is done in Ref. [25] which writes the scaling along with the smallest correction term:

$$\begin{aligned}\log M &= \mathrm{Log}A + D_f \log L + \log(1 + aL^{-\omega}) \\ &\approx \mathrm{Log}A + D_f \log L + aL^{-\omega}.\end{aligned} \tag{6}$$

Thus, rather than fitting to a line in a log-log plot one fits to (5) or (6) (gave comparable results) and simultaneously finds the best D_f, ω. We found this technique to produce marginal success but still found evidence of finite-size effects. Instead, we chose to directly reproduce (3) by extracting the local fractal dimension for lattices in a range of sizes $[50, 10^4]$ and fitting the asymptote directly. The results are shown in Fig. 3.

In order to determine whether SIP and BIP share the same universality class, one must determine at least two of the scaling parameters. From these, all others can be determined. A common measure is the percolation backbone which is closely related to the transport properties of a sample-spanning cluster. The backbone is defined to be the subset of the cluster which has all dangling ends removed (ends not in contact with the lattice boundary). It serves as a measure of conductivity, since it is the set of paths through the lattice if one begins on one boundary side and ends at another. The backbone is characterized by the path distance, D, of the connected sites composing the backbone, and the lattice size L which hosts the cluster according to:

$$D(L) \sim L^{D_{bb}}. \tag{7}$$

A closely related quantity is how the distance between two arbitrary lattice points scale in terms of lattice site spacing l. This follows another power law:

$$M(l) \sim l^{D_l}, \tag{8}$$

where $M(l)$ is the number of sites within lattice spacing l and D_l is the chemical dimension [27]. With backbone studies one must be more careful with how boundary conditions are imposed (periodic, etc.). Thus it is preferable to use D_l which is largely independent of such affects. Further, what we are really interested in is characterizing the compactness of a cluster which describes the types of paths connecting sites. We can relate the Pythagorean distance r and l as:

$$l \sim r^{D_{\min}}. \tag{9}$$

Therefore if d is the path distance from the origin to the boundary of lattice size L, then $L = nl$ and by Eq. (9) we can write:

$$d \sim r^{D_{\min}}, \tag{10}$$

where $D_{\min}$ is the fractal dimension of the shortest path. A peculiar affect is how diffusion slows near criticality because

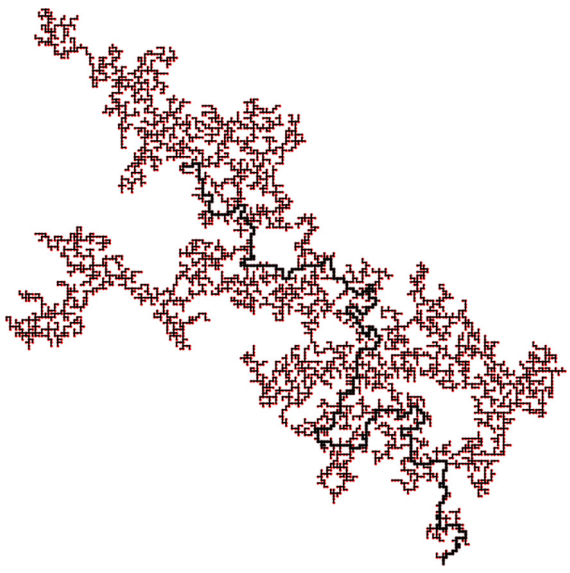

FIG. 4. An example of a typical path (darkened line segment) produced by the LSIP algorithm. We use a recursive algorithm to find the path from the injection site to the the end of cluster. The end of the cluster is defined to be the site of the lattice boundary.

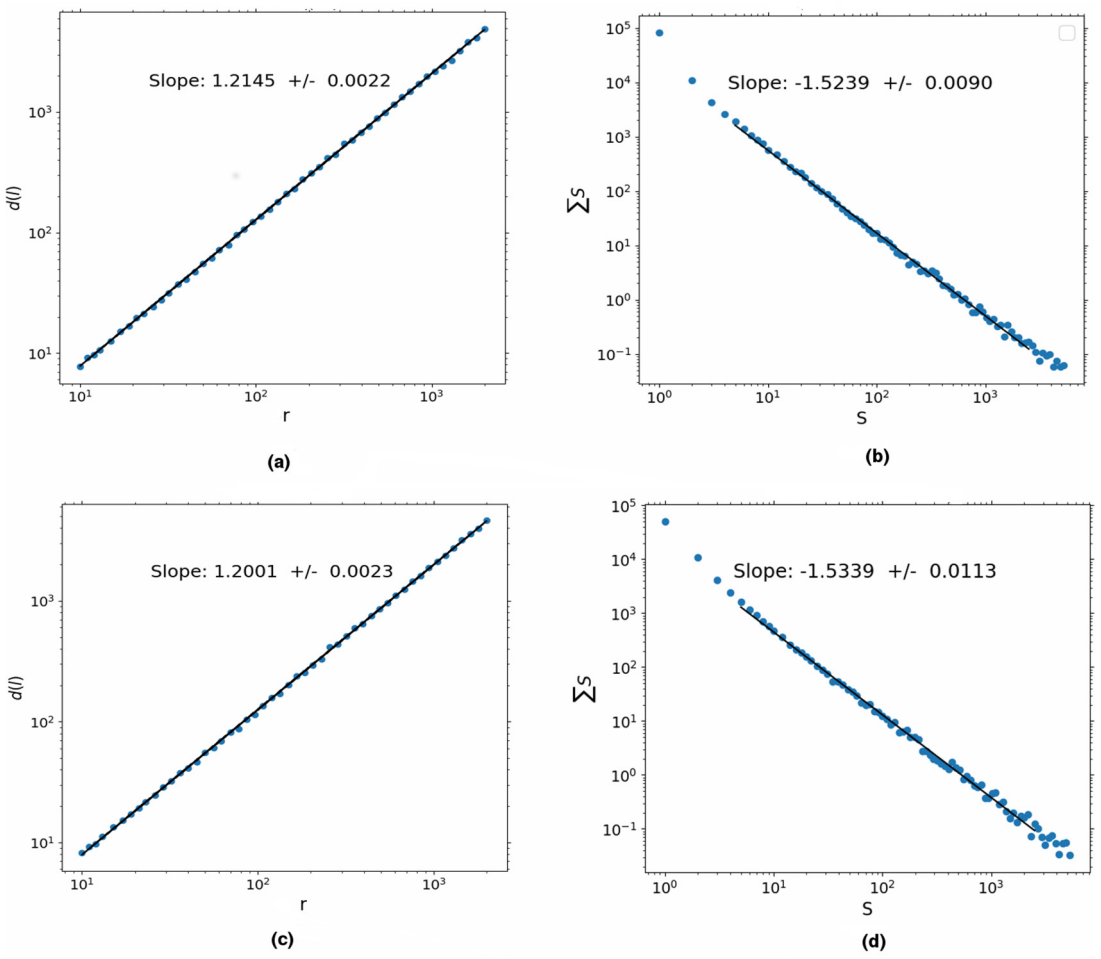

FIG. 5. $D_{\min}$ and τ characterization for LSIP and LBIP. Plots (a) and (c) are a log-log plot of an ensemble average of the path distance between sites, $d(l)$, where the lattice spacing between sites is l. We averaged over 100 samples for each L in the range [10,2000]. Plots (b) and (d) show the burst magnitude-frequency scaling for LSIP and LBIP respectively. For each, we generated ≈120 000 bursts which ranged from size 1 to $\sim 4 \times 10^3$. We binned the counts of each burst size (blue dots) using log sized bins in order to extend the fit data range. The fits were all done via minimization of least squares.

the sizes of the holes in the cluster become scale invariant, thus allowing holes of all sizes to form. The paths are then forced to become more circuitous. Because the IP process is always critical, we expect the path length to follow Eq. (10).

To determine the path length described by Eq. (10), we make use of the loopless condition which allows us to reorganize the cluster of connected sites into a tree. We show an example of the shortest path for LSIP in Fig. 4. Since there only exists a single path between two points this path trivially represents the shortest path between two points, we use recursive search routines to find paths between sites much more efficiently. We create an ensemble of clusters with lattice size L in range [10, 2000] and calculate the path length from the origin to the boundary. The results are shown in Fig. 5 where we find $D_{\min} = 1.215 \pm 0.002$ and $D_{\min} = 1.200 \pm 0.002$ for LSIP and LBIP, respectively.

The loopless condition simplifies the paths within our clusters since there can only be one. Absent recursive methods, path search algorithms can take more time finding paths between sites than creating the original cluster. Also, this simplification creates paths with other applications like the paths which resembles domain walls in the strong disorder limit of spin glass systems [28]. The paths also resemble Prim's algorithm for finding the shortest spanning tree of a weighted random graph. It represents the minimum energy tree spanning all vertices [29].

IV. BURST CHARACTERIZATION

Physically, we think of a burst in our model as a rapid accumulation of filled sites which corresponds to a formation of sublattice regions having different permeability or conductivity from which the sublattice originates. In fracking, these would be the regions where the stress field rapidly changes and hosts the observed microseismicity. Our burst model must then follow a power law, and we also expect to reproduce similar spatial distribution of burst centers to the epicenters of earthquakes from fracking.

IP was intended to simulate the quasistatic displacement of one fluid by another through capillary forces. The networks produced simulate long time expectations of systems eventually able to achieve equilibrium. Though at each iteration a site is invaded or a bond breaks, the network characteristics

are loosely coupled to these details (as we see SIP and BIP sharing nearly identical network characteristics). While there does not seem to be inherent time dynamics in IP models, different attempts have been made to understand or uncover inherent time dynamics Furuberg *et al.* [30].

These authors examined the dynamics that arise when a time step corresponds to the invasion of a single site. They found $r \sim t^{1/D}$, which we expect since here t is also the number of invaded sites or has the equivalent interpretation as being the mass (number of invaded sites) for a cluster with size r. Here D is the fractal dimension of the SSC and in the limit where the fractal dimension ∼2 (an SSC completely filling all sites of a lattice) we recover the results of distance traveled in a diffusion process.

If paths can only traverse filled sites, then a lower fractal dimension will mean a more sparsely filled lattice which will limit potential trajectories on the lattice. The result is that we recover the path length of a random walk on typical percolation cluster. The authors took this relation to mean that at time t, most of the region within r is likely already invaded, and it is unlikely to have growth at distances larger than r. Their notion of a burst was that in time t, growth can be found to be in some distance r. Yet, it seems this is merely restatement of the behavior of a random walk on a percolation cluster and does not introduce any true burst dynamics.

Much of the dynamics associated with IP has to do with the transport exponents which are mostly governed by the kinds of paths which can form through the percolating cluster. However, RP does follow a cluster size scaling law described by the Fisher exponent, τ:

$$n_s(p) = s^{-\tau} f[(p - p_c)s^{\sigma}], \tag{11}$$

where for $(p \to p_c)$, the cluster size,$n_s(p) \sim s^{-\tau}$. So, there is credence to the idea that a network can grow in bursts if IP grows its SSC by different realizations of these RP clusters.

The growth algorithm for IP is different from RP since IP will always grow indefinitely and further exhibits a kind of self-organized criticality, since the cluster will grow by a self-organized selection of bonds strengths less than the critical probability. Reference [33] defined a notion of a burst resulting in a power law similar to that of RP when $(p \to p_c)$. The authors showed that if we consider the sequence of broken bonds to be a signal $x(t)$ [where $x(t)$ is the bond strength broken at time t], then over some signal length $x(t + s)$, there will be a sequence of bonds broken. For all t' in range $t < t' < t$, the bond strengths broken, $x(t')$, will be $x(t) < x(t') < x(t + s)$.

The number of bonds broken in time range $(t + s)$ can be made to follow a power law if the threshold strength of $x(t)$ is chosen to be near the critical probability as was also shown by authors in Ref. [20]. That is, IP clusters will grow by a self-organized selection of bonds strengths less than the critical probability, but if the threshold is chosen to be near the critical probability, the SSC will grow in iterations of clusters similar to those of RP though with a different value for the Fisher exponent. In particular, from Fig. 6 we see that if the threshold, $T \sim p_{\text{crit}}$, then the average burst size exhibits critical behavior. Choosing our threshold to be in this range

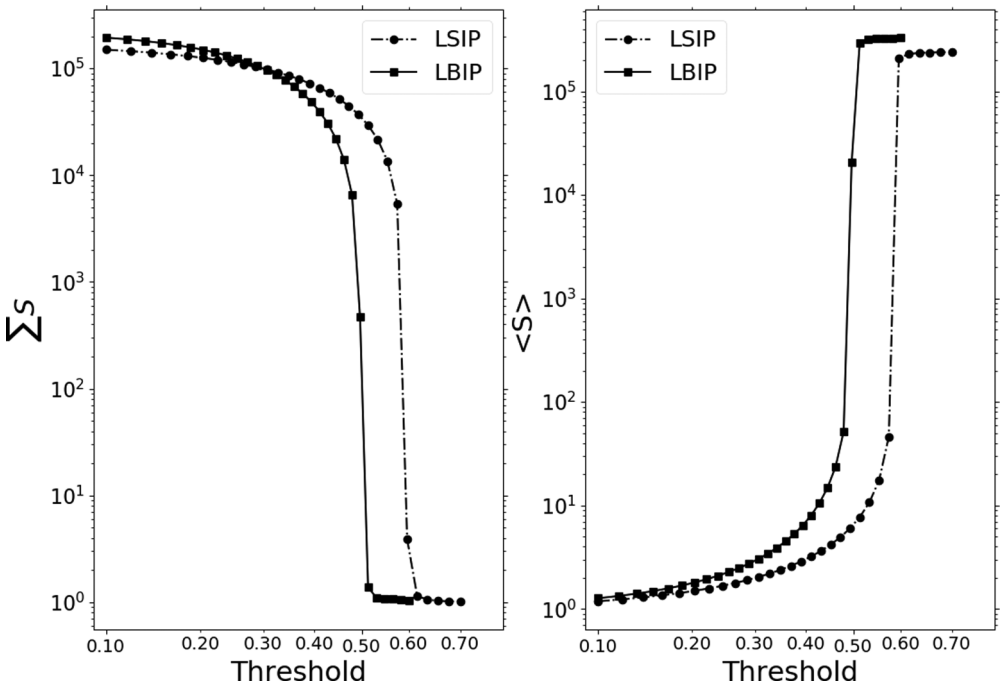

FIG. 6. Critical behavior of LSIP and LBIP. Utilizing our notion of a burst, there exists a particular threshold where the average size of a burst, $\langle S \rangle$, behaves critically for LSIP and LBIP. This value corresponds to the critical occupation probability, p_{crit} for BIP and SIP which is known to be 0.5 and ∼0.592, respectively. The left plot, shows how the number of bursts decreases to 1 if the threshold, $T > p_{\text{crit}}$. Similarly, the right plot shows how the average burst size, $\langle S \rangle$, grows to include all sites if the threshold $T > p_{\text{crit}}$. If the threshold $T \sim p_{\text{crit}}$, then our burst magnitude frequency distribution will follow a power law with b value ∼1.54.

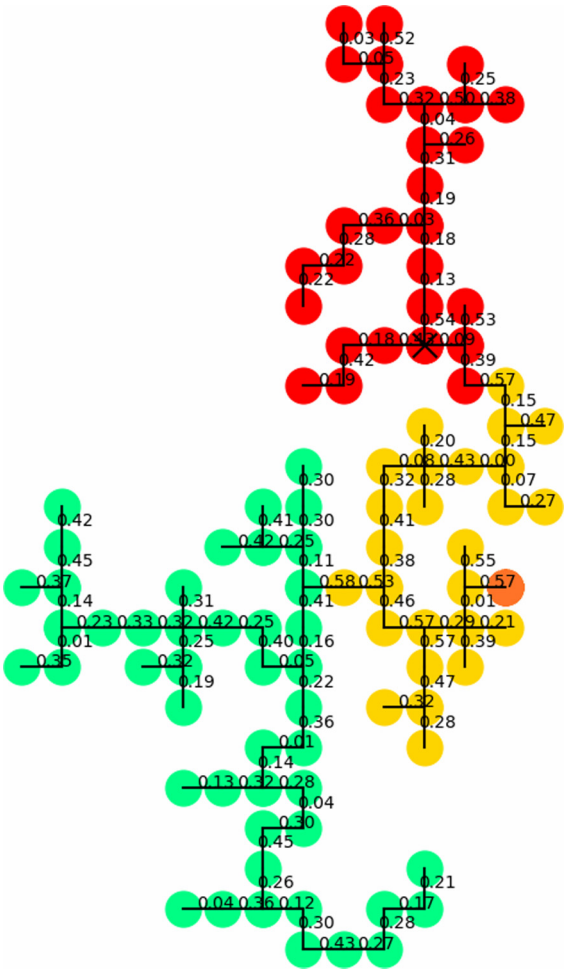

FIG. 7. Avalanche tree burst example for SIP with a burst threshold set to be $T = 0.57$ near $p_c = 0.59$. Each burst is shown by a different color, where the injection site is marked by "×" in the red burst and migrated to the yellow, blue, and green. The bond strengths are shown to illustrate all the sequence of connected bonds with strength less than T belong to the same burst.

will result in a burst-size frequency distribution that is scale invariant and reproduces a power law.

In addition to this choice of burst threshold, we demand that our bursts be spatially connected in addition to sequentially (previous studies only demanded sequentially connected bonds or sites [20,33]). Our bursts should only be allowed to grow from the local percolation front of a burst rather than the global percolation front from the entire cluster. Since our networks are necessarily loopless, we can utilize the tree structure to define sequentially and spatially connected bursts in a very natural way.

Again, the critical aspect of a burst is that it should fill up a certain portion of a lattice until it exhausts all the easiest bonds. Once a strong bond is forced to break, a new region of weak bonds should become available, allowing a quick succession of bonds to break. The successive breaking of weaker bonds below a threshold defines a burst. Again, because a percolation cluster has no intrinsic time dynamics, we are free to retroactively say how the tree grew and that it in fact grew in bursts.

Figure 7 shows how a cluster can be divided into different colored subtrees where each subtree is made to corresponds to a burst. The tree structure advantage is that one can define a burst to be its own subtree which connects at only one point to the original tree. The process of determining bursts becomes a process of cutting a single tree cluster into a collection of subtrees, all of which are connected to each other through only 1 node (i.e., a similar connectedness criteria as before).

To define a burst we then traverse the tree from the origin until we exhaust all bonds less than the threshold strength; we cut the tree at this point, and define this cut point to be the root node of the subsequent tree. The process continues again traversing all the nodes weaker than the threshold strength. A similar mechanism is used to explain the opening of bronchial airways in lungs [34]. We note that generalized avalanche models on trees also follow power laws [35].

V. RESULTS

Detailed studies of fluid injection into a porous medium on the pore scale reveals very complex behavior. This is largely the result of porous medium morphology being itself highly disordered and random [36]. Therefore a statistical characterization seems appropriate and it is this characterization these (invasion) percolation models aim to reproduce. Within percolation theory we can model fluid displacement as two different processes. The process by which a fluid is drawn into a network of pores is imbibition, whereas a nonwetting fluid forced into porous volume is drainage. We model these as SIP and BIP, respectively, and it is our primary interest to determine if HF is better described by one of these processes. In doing so, we might gain insight into the appropriate physics at the individual pore scale. Otherwise, it demonstrates our sensitivity to the dynamics at different scales.

Since the scaling exponents which characterize the universality class are the same as those used to constrain our model via observed microseimicity, a closely related question is whether SIP and BIP share the same universality class. While we find small differences between the two models which does suggest unique universality classes, the differences are sufficiently small to suggest that we do not have sensitivity in

TABLE II. A comparison of scaling exponents for loopless site invasion percolation (LSIP), loopless bond invasion percolation (LBIP), random percolation (RP), loopless random percolation (LRP), nontrapping site invasion percolation (NTSIP), trapping bond invasion percolation (TBIP), and diffusion limited aggregation (DLA).

	D_f	$D_{\min}$	τ
LSIP (this paper)	1.902±0.003	$1.215 \pm .002$	$1.524 \pm .009$
LBIP (this paper)	1.945±0.009	$1.200 \pm .002$	$1.534 \pm .011$
RP [25]	$91/48 \approx 1.896$	1.13 ± 0.004	$187/91 \approx 2.05$
NTSIP [31]	1.8959±0.0001	1.1307 ± 0.0004	—
TBIP (square lattice) [31]	1.822±0.008	1.214 ± 0.002	—
DLA [32]	1.69±0.24	1.0 ± 0.02	—

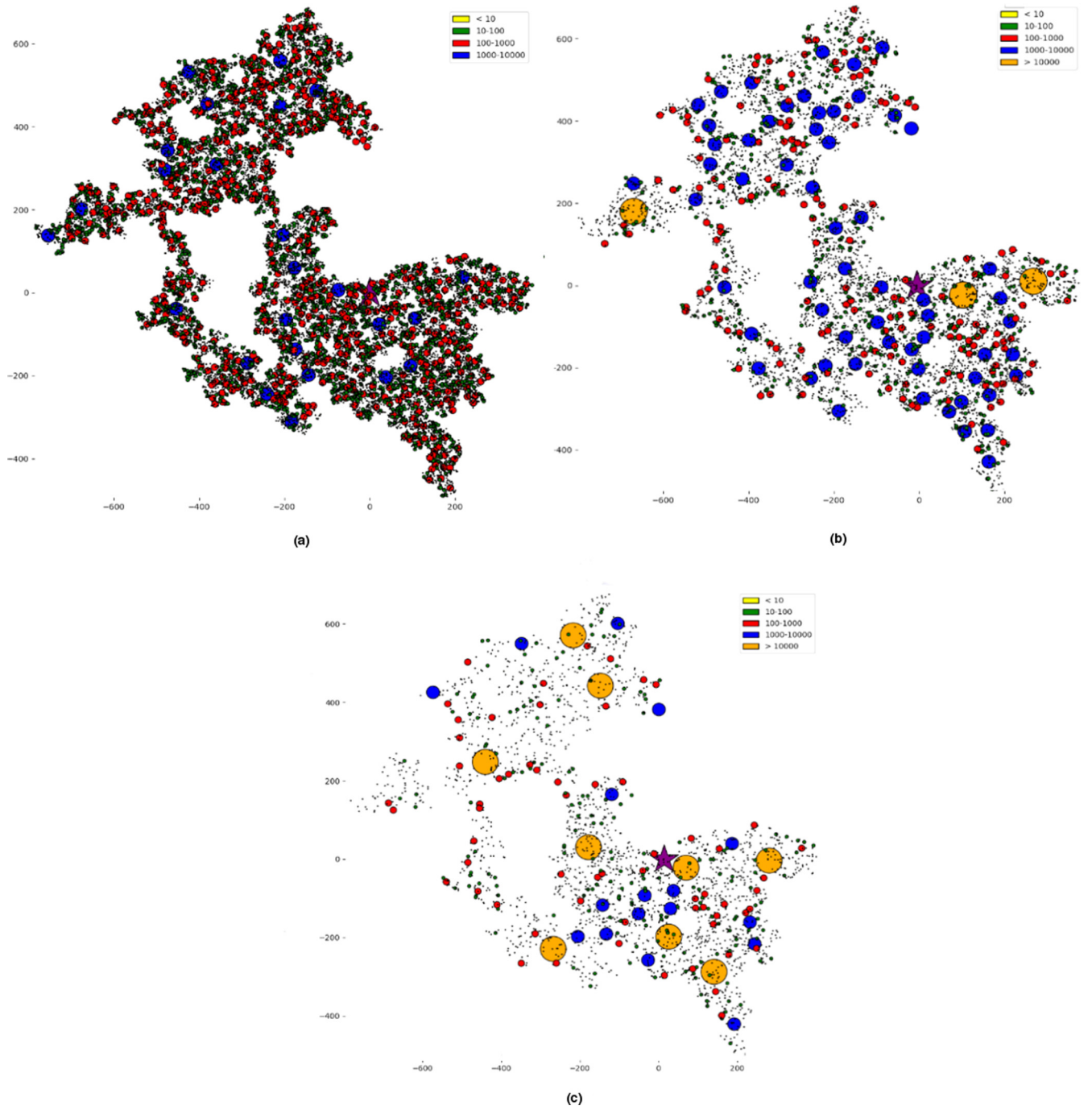

FIG. 8. An example of a SSC containing 300 000 bonds broken into its separate bursts according to the burst threshold. The bursts are shown where each burst is drawn as a circle with size proportional to the number of broken bonds and the bursts location determined by the bursts' center of mass. The plots (a), (b), and (c) are a comparison of how the burst size distribution changes as the burst threshold changes ($T = [0.45, 0.48, 0.49]$), respectively, and approaches the critical probability, $p_{\text{crit}} = 0.5$. The sizes of the bursts tend to a power-law distribution as the threshold tends to the critical probability. The purple star indicates the injection site of the entire cluster.

data to distinguish between the two. Table II shows our values along with their observed error.

There seems to be many conflicting values for the scaling exponents in the literature. We believe a major reason for this is inadequate treatment of finite-size effects. Even large lattices with large SSC's with 10^7 sites can have significant finite-size effects (as seen in Figure 3 where a lattice size of 10^4 has $\sim 10^7$ sites). We find evidence that in the limit of infinite lattice size, the fractal dimension of SIP approaches the expected value of RP.

For BIP, which seems to be more compact than SIP at all lengths scales approaches a value of $D_f = 1.945 \pm 0.009$. This value is different from SIP, which has value $D_f = 1.902 \pm 0.003$. Figure 3 very clearly shows how the "local" fractal dimension can change as a result of the lattice size.

We find that because LBIP is more compact, there is a small difference in the value of $D_{\min}$ as described by Eq. (10). The fractional dimension $D_{\min}$ was found to be $D_{\min} = 1.215 \pm 0.002$ and $D_{\min} = 1.200 \pm 0.002$ for LSIP and LBIP, respectively. Results from the literature for $D_{\min}$ are 1.2138 [20], 1.2 ± 0.02 [29], 1.22 ± 0.01 [28], 1.23 ± 0.02 [37], and 1.214 ± 0.001 [38]. Regular percolation gives $D_{\min} = 1.13$ and a random walk has $D = 1.19$.

The scaling of the burst magnitude-frequency distribution allows us to compare how well our bursts reproduce the scaling associated with fracking microseismicty. We find that despite small differences in their other scaling exponents, our models produce the same magnitude-frequency distribution with their respective errors ($\tau = 1.524 \pm 0.009$, $\tau = 1.53 \pm 0.01$ for LSIP and LBIP respectively). Fig. 8 gives an example of how our model of bursts near criticality and our simulated fracture network produces a representation of the expected microseismicity within a region.

Our burst scaling is compatible with that observed during induced seismicity and is significantly different from the b-value of typical tectonic earthquakes. In order to account for the variability of b values associated with induced microseisimicity we find that for thresholds $T < p_c$, we can produce burst statistics which prefer smaller earthquakes, suggesting that induced microseismicity may not be characterized by critical phenomena unlike tectonic seismicity which is known to be critical [17].

In order to maintain generality we emphasized maintaining model simplicity. Further, because we believe most of the observed HF seismicity is the result of critical phenomena, only a subset of system behavior becomes relevant. This subset being the nature of the inherent randomness and how it grows to all scales of the system. Our statistical approach means we avoided introducing much of the local environment conditions which have a large affect on individual realizations of induced miscroseismicity. Most notably the spatial distribution of the epicenters of earthquakes seem to depend on the local stress field and fracture network. This produces seismicity which uniquely clusters in some regions and is rather isotropic in others.

This study shows that this approach can reasonably reproduce HF seismicity's essential statistics and serves to illustrate the sensitivity to small-scale physics one can hope for with such an approach.

Our models produce isotropic spatial distribution of bursts and can therefore only account for some of the observed features. It is known that pore sizes within rocks are not independent and random but rather exhibit correlations. Since we are insensitive to distinctions between pore or bond dynamics, by introducing correlations in pore sizes, we should be able to more accurately describe fracture networks and better account for the variations of induced microseismicity. This will be the subject of future work.

ACKNOWLEDGMENTS

The research of R.A.O. and J.B.R. has been supported by a grant from the US Department of Energy to the University of California, Davis, DOE Grant No. DE-SC0017324.

[1] D. Wilkinson and J. F. Willemsen, J. Phys. A: Math. Gen. **16**, 3365 (1983).
[2] C. P. Stark, Nature (London) **352**, 423 (1991).
[3] J. T. Clemmer and M. O. Robbins, Phys. Rev. E **100**, 042121 (2019).
[4] J. P. Stokes, A. P. Kushnick, and M. O. Robbins, Phys. Rev. Lett. **60**, 1386 (1988).
[5] K. J. Måløy, S. Santucci, J. Schmittbuhl, and R. Toussaint, Phys. Rev. Lett. **96**, 045501 (2006).
[6] S. Maxwell, Lead. Edge **30**, 340 (2011).
[7] F. Ebrahimi, Comput. Sci. Eng. **12**, 84 (2010).
[8] M. M. Scuderi and C. Collettini, Sci. Rep. **6**, 24852 (2016).
[9] M. Scuderi, C. Collettini, and C. Marone, Earth Planet. Sci. Lett. **477**, 84 (2017).
[10] M. Sahimi, M. C. Robertson, and C. G. Sammis, Phys. Rev. Lett. **70**, 2186 (1993).
[11] J. B. Rundle, J. Geophys. Res.: Solid Earth **94**, 12337 (1989).
[12] B. E. Shaw, Geophys. Res. Lett. **20**, 907 (1993).
[13] Y. Y. Kagan, Geophys. J. Int. **168**, 1175 (2007).
[14] J. Henderson, D. Barton, and G. Foulger, Geophys. J. Int. **139**, 317 (1999).
[15] R. Chandler, J. Koplik, K. Lerman, and J. F. Willemsen, J. Fluid Mech. **119**, 249 (1982).
[16] K. Aki, Earthquake Prediction: Int. Rev. **4**, 566 (1981).
[17] J. B. Rundle, R. Ortez, J. Kønigslieb, and D. L. Turcotte, Phys. Rev. Lett. **124**, 068501 (2020).
[18] M. Luginbuhl, J. B. Rundle, A. Hawkins, and D. L. Turcotte, Pure Appl. Geophys. **175**, 49 (2018).
[19] M. Sahimi, M. Hashemi, and J. Ghassemzadeh, Physica A **260**, 231 (1998).
[20] J. Q. Norris, D. L. Turcotte, and J. B. Rundle, Phys. Rev. E **89**, 022119 (2014).
[21] A. Kantzas and I. Chatzis, Chem. Eng. Commun. **69**, 191 (1988).
[22] M. Porto, S. Havlin, S. Schwarzer, and A. Bunde, Phys. Rev. Lett. **79**, 4060 (1997).
[23] H. E. Stanley, *Introduction to Phase Transition and Critical Phenomena* (Oxford University Press, Oxford, 1971).
[24] S. Havlin and A. Bunde, *Fractals in Science* (Springer-Verlag, Berlin 1994).
[25] D. Stauffer and A. Aharony, *Introduction to Percolation Theory*, 2nd ed. (Taylor & Francis, London, 1994).
[26] M. A. Knackstedt, M. Sahimi, and A. P. Sheppard, Phys. Rev. E **61**, 4920 (2000).
[27] S. Havlin and R. Nossal, J. Phys. A: Math. Gen. **17**, L427 (1984).
[28] M. Cieplak, A. Maritan, and J. R. Banavar, Phys. Rev. Lett. **72**, 2320 (1994).
[29] A.-L. Barabási, Phys. Rev. Lett. **76**, 3750 (1996).
[30] L. Furuberg, J. Feder, A. Aharony, and T. Jøssang, Phys. Rev. Lett. **61**, 2117 (1988).
[31] M. A. Knackstedt, M. Sahimi, and A. P. Sheppard, Phys. Rev. E **65**, 035101(R) (2002).

[32] P. Meakin, I. Majid, S. Havlin, and H. E. Stanley, J. Phys. A: Math. Gen. **17**, L975 (1984).
[33] S. Roux and E. Guyon, J. Phys. A: Math. Gen. **22**, 3693 (1989).
[34] B. Suki, Nature (London) **368**, 615 (1994).
[35] L. P. Kadanoff, S. R. Nagel, L. Wu, and S.-m. Zhou, Phys. Rev. A **39**, 6524 (1989).
[36] M. Sahimi, *Flow and Transport in Porous Media and Fractured Rock: From Classical Methods to Modern Approaches* (John Wiley & Sons, New York, 2011).
[37] J. Mastorakos and P. Argyrakis, Phys. Rev. E **48**, 4847 (1993).
[38] A. P. Sheppard, M. A. Knackstedt, W. V. Pinczewski, and M. Sahimi, J. Phys. A: Math. Gen. **32**, L521 (1999).